

DOI: 10.7641/CTA.2013.12049

基于旋转分类模糊纹理谱的矿物浮选泡沫平滑度分析

周璇, 阳春华, 任会峰[†], 陈志鹏, 曾子骄

(中南大学信息科学与工程学院, 湖南长沙 410083)

摘要: 矿物浮选的精矿品位与泡沫的纹理复杂度密切相关. 为了避免纹理谱方法中像素值的刚性比较, 提出了一种新的基于旋转分类模糊纹理谱的纹理描述方法用于金属矿物分离. 经过指数函数拟合频率分布曲线, 确定模糊阈值大小, 统计模糊纹理单元, 给出了灰度差值的模糊纹理谱, 并利用旋转分类将 6561 种纹理单元简化至 834 种. 基于此, 引入 2 个描述因子, 纹理平滑度与粗糙度. 实际应用结果表明, 纹理平滑度可描述图像纹理粗糙程度, 同时反映实时矿物品位.

关键词: 泡沫浮选; 纹理特征; 模糊控制; 旋转分类; 机器视觉

中图分类号: TP29 文献标识码: A

Froth homogeneity analysis using rotate classification fuzzy texture spectrum for mineral flotation process monitoring

ZHOU Xuan, YANG Chun-hua, REN Hui-feng[†], CHEN Zhi-peng, ZENG Zi-jiao

(School of Information Science and Engineering, Central South University, Changsha Hunan 410083, China)

Abstract: The concentration grade in mineral flotation is closely related to the froth texture complexity. To deal with the defects of rigid comparison of basic texture spectrum, we present a novel rotate classification fuzzy texture spectrum method for mineral separation process from engineering aspects. The frequency-statistics curve of neighborhood pixels grayscale difference is fitted by using an exponential function, and the optimal threshold value of the fuzzy internal is determined. According to the grayscale difference between neighborhood pixels and seed pixel in local region, the fuzzy texture unit is constructed, which is used to calculate the fuzzy texture spectrum of various fuzzy texture unit numbers. Meanwhile, the original 6561 texture units are simplified to 834 classes. The homogeneity and the coarseness are introduced to describe the froth texture feature. The analysis results of froth images with different grades in spot show that the texture homogeneity can reflect the concentration grade in real-time.

Key words: froth flotation; texture feature; fuzzy control; rotate classification; computer vision

1 Introduction

Copper, aluminum, lead, zinc and other metals are closely related to human life. However, as the consumption is growing gradually, corresponding mineral resources are diminishing. At present, most of the existing ores are lean or symbiotic mine, so it's severely significant to extract and recycle the valuable metals effectively. Froth flotation is the application of surface science to separate and purify valuable minerals from gangue according to different hydrophobic of the surface properties of various minerals^[1-2]. Because of its great adaptability and high efficiency, it now becomes the most widely used method of separation and purification of the low grade or complex ore^[3-4]. In recent years, flotation has been extended to medical and health, environmental protection^[5], resource recycling^[6] and many other fields.

Researches have shown that visual characteristics of the surface froth in flotation cell are the comprehensive reflection of mineral physical properties, flotation reagents, and mechanical and operating conditions^[7]. With the advantages of computer science and image processing tech-

nology, computer-vision is widely used in industry process monitoring^[8-10]. Experts studied bubbles color^[11-13], size^[14-15], velocity^[16], and other features^[17-18] of flotation froth under computer-vision, deduced the relationships between bubbles appearance and flotation performance^[19-21].

The homogeneity of bubbles surface can be described by image texture, which can reflect the enrichment of mineral on the froth, so the froth texture tied to concentrate grade closely^[22]. Marais^[23] and Aldrich^[24] studied the texture of froth based on gray level co-occurrence matrix (GLCM) and proved the relationship between mineral grade and recovery. But GLCM is beyond the model of human vision, and the global use of information is missing. Hyötyniemi has extracted the froth texture based on GGHA and power spectrum using fast fourier transform (FFT)^[25]. However this method is compute-intensive for simulation only. Bartolacci used Wavelet to extract texture features of froth images^[20]. But the Wavelet method for extraction of texture quality is limited to the selection of filter bank issues. The requirement of multiple filter banks causes a number of parameters need to be deter-

Received 9 March 2012; revised 17 May 2013.

[†]Corresponding author. E-mail: renhf316@163.com; Tel.: +86 13548681086.

This work was supported by the National Natural Science Foundation of China (No.61134006), the National Science Foundation for Distinguished Young Scholars (No.61025015), and Foundation Sciences Central South University.

mined, which is not conducive to real-time estimation of the parameters. Holtham^[26] and Lin^[27] once used basic texture spectrum (BTS) to predict the bubble size, but the BTS considers only the rigid comparison of the adjacent pixels, and cannot discriminate the difference from less, far less or greater and far greater than. Then a Fuzzy Texture Spectrum method is proposed by Cheng Cui-lan^[28] which solved the problem but raise another problem of calculation dimensionality and computer efficiency.

The remainder of this paper is organized as follows: The second section of the paper outlines the basic process of bauxite froth flotation and the acquisition equipment of froth images. The characteristic of bauxite froth is also discussed. The third section presents the rotate classification texture spectrum and rotate classification fuzzy texture spectrum. Section 4 gives the coarse and homogeneous membership function based on rotate classification fuzzy texture spectrum. Computational results for numbers of froth images acquired in spot are discussed in the fifth section. Finally we make a conclusion with a direction for further investigation in Section 6.

2 Froth image acquisition and analysis

Froth flotation is a complex physical-chemical reaction process with gas, liquid, solid-phase interaction^[29]. As shown in Fig.1, various reagents are injected into the flotation cell, and mixed with the micron powder minerals and industrial water to form slurry. The impeller driven by belt pulley rotates at a high speed. Air flow is divided into numerous tiny bubbles under the role of vortex and the cross movement of the pulp and the airflow. During rising, bubbles can glue the hydrophobic valuable mineral to the surface of flotation cell. The froth on the surface is recycled to cell lip as concentrate via scraper. While hydrophilic gangue minerals retain in the pulp and discharge as tailings.

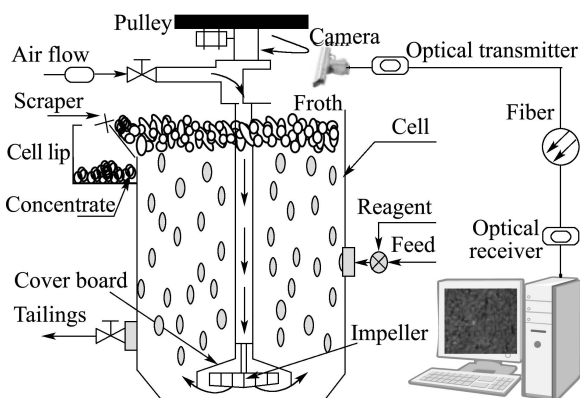


Fig. 1 Diagram of froth image acquisition system

Fig.2 is the photo of froth image acquisition device for mineral flotation in spot.

The specification of flotation cell is XCF-KYF-40, whose effective volume is 40 m³. A color CCD camera is positioned 110 cm above the froth surface. Because the characteristics of froth is affected by the surface turbulence caused by scraper while blowing, the camera should be installed far away from the cell lip, which meanwhile guarantees it captures fresh froth images. The fluorescent lamp

with high brightness and stable color temperature lights for the camera. Its installation position should be a little higher than the camera and make sure there is no camera's projection falling in the view of camera. Camera is chosen with a vision field of 12.8×9.6 cm² and a shooting rate of 7.5 frames per second. The image size is set at 800×600 pixels. Video signal through fiber cable is transferred to an industrial computer and digitized by an image acquisition card to display online.

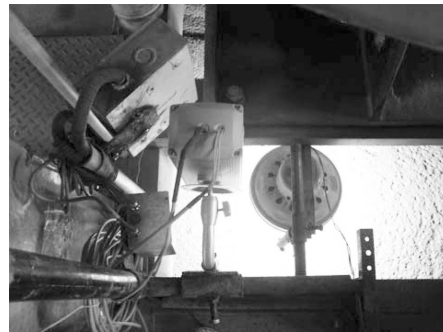


Fig. 2 Hardware device for froth image acquisition

At present, flotation is mainly about sulphide ore of heavy metals such as copper, lead, zinc etc..Compared to light metals, there is less bubbles accumulation, less extrusion deformation, larger bubbles, and more clear bubble border for heavy metals, rendering calculation of their morphology information easy and dependable. This paper is about bauxite, whose main ingredient is diaspora, belonging to light metal oxide. The oxygen-containing anions (or ion) in bauxite are easily integrated with water molecules to form hydrogen bonds, which has strong water affinity and small wetting contact angle^[30]. Fig.3 is a froth image acquired on field. As can be seen, the perspective of the camera is full of extruded bubble cascade without reference background. The bubbles come in all shape. Moreover the froth image has uneven highlight distribution on the surface, blurry boundaries and ambiguous top highlights, looking like batting. In addition, the turbulence due to high speed rotation of the impeller and the scraper movement makes it difficult to accurately extract the bubble's morphological characteristics such as size, shape, and velocity. Thus, texture is relatively robust and much more practical and efficient to analyze this kind of froth.

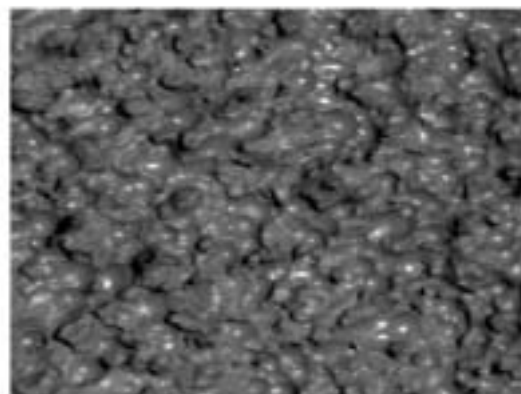


Fig. 3 Froth image

3 Fuzzy texture spectrum

3.1 Texture spectrum

A bubble image can be seen as constituted by many of the 3×3 regions. Assume V_i is the gray scale of i th pixel within the region. Central pixel V_0 is called as seed pixel, V_1 - V_8 as neighboring pixels^[31].

Texture unit vector $TU = (E_1, \dots, E_8)$ is defined as following formula:

$$E_i = \begin{cases} 0, & \text{if } V_i < V_0, \\ 1, & \text{if } V_i = V_0, \quad i = 1, 2, \dots, 8. \\ 2, & \text{if } V_i > V_0, \end{cases} \quad (1)$$

The 3×3 region is called a texture unit. According to (1), each E_i in texture unit vector has 3 possible values. Then calculate V_1 - V_8 from top left corner along clockwise, there are $3^8 = 6561$ different texture unit vectors, which can be discriminated using the variable-texture unit number(N_{TU}), ranging from 0 to 6560, calculated as (2):

$$N_{TU} = \sum_{i=1}^8 E_i \times 3^{i-1}. \quad (2)$$

All of the pixels in froth image are individually scanned, the TU of which are labeled in turn. By computing N_{TU} , the frequency of all N_{TU} is defined as texture spectrum and represented as histograms. Therefore N_{TU} is a local description of the texture, whereas texture spectrum is a global description. In addition, according to the definition of texture unit vector, that all of E_i equal to 1 ($N_{TU} = 3281$) shows there are exactly the same gray scale of 9 pixels in the 3×3 region. Then the local area of froth is smooth. The more 0 or 2 there are, the coarser the froth image is.

3.2 Fuzzy texture spectrum(FTS)

As can be known from the above parts, BTS which is using a rigid comparison of gray scale between neighborhood pixels and the seed pixel, cannot discriminate the difference from less, far less or greater and far greater than. For example, Fig.4 (a) and (b) varies, but according to the BTS, we get the same texture unit, whose N_{TU} is 4898, shown in Fig.4(c). To distinguish the difference, fuzzy algorithm is proposed here. Define fuzzy texture unit as texture box consisting of fuzzy sets (μ_0, μ_1, μ_2) , where μ_i means the probability of the gray scale of neighborhood pixel being less, equal to or greater than the seed pixel^[32].

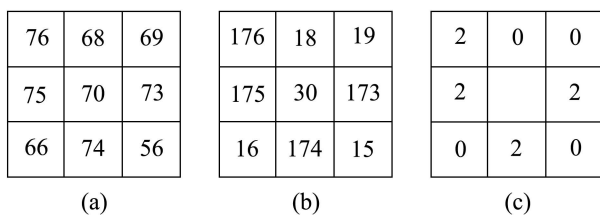


Fig. 4 Texture unit of different region

Fuzzy rules given as below:

Rule: The grayscale difference of neighborhood pixels V_i and seed pixel V_0 is denoted as d^i . The smaller d^i is, the greater probability of V_i equaling to V_0 , and vice verse.

For example, a 512×512 pixels area is cropped in Fig.3. After the grayscale difference statistic of adjacent

pixels, the curve of grayscale difference frequency is fitted by exponential function. As shown in Fig.5, the solid line is the statistics curve, while the dashed line is the exponential approximation curve. In Fig.5, the probability of $|d^i| > 4$ is less than 0.1, to simplify the calculation, we regard their possibility of equal as 0. Therefore, the exponential type membership function can be defined as Equations (3)–(5):

$$\mu_0(d^i) = 1 - \mu_1(d^i) = \begin{cases} 1, & \text{if } d^i \leq -4, \\ 1 - 1.45^{d^i}, & \text{if } -4 < d^i < -1, \\ 0, & \text{if } d^i > -1, \end{cases} \quad (3)$$

$$\mu_1(d^i) = \begin{cases} 0, & \text{if } |d^i| \geq 4, \\ 1.45^{-|d^i|}, & \text{if } 1 < |d^i| < 4, \\ 1, & \text{if } -1 \leq d^i \leq 1, \end{cases} \quad (4)$$

$$\mu_2(d^i) = 1 - \mu_1(d^i) = \begin{cases} 0, & \text{if } d^i \leq 1, \\ 1 - 1.45^{-d^i}, & \text{if } 1 < d^i < 4, \\ 1, & \text{if } d^i \geq 4. \end{cases} \quad (5)$$

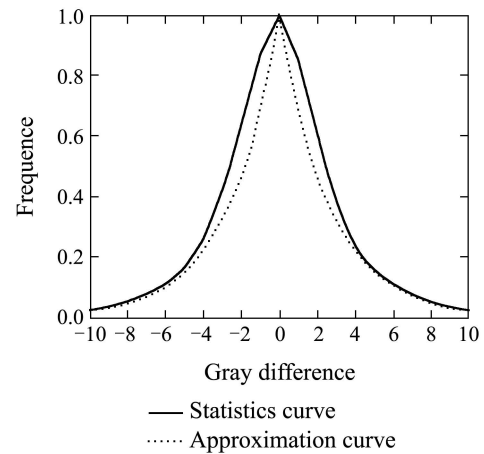


Fig. 5 Grayscale difference frequency statistics of adjacent pixels

As in Fig.4, the FTS calculation of (a) is shown as following while the FTS calculation of (b) retains.

Texture unit number and its probability of the fuzzy texture unit in Fig.6 are in Table 1.

$(0_0 \ 1_0 \ 2_1)$	$(0_{0.6914} \ 1_{0.3086} \ 2_0)$	$(0_0 \ 1_1 \ 2_0)$
$(0_0 \ 1_0 \ 2_1)$		$(0_0 \ 1_{0.1715} \ 2_{0.8285})$
$(0_0 \ 1_0 \ 2_0)$	$(0_0 \ 1_0 \ 2_1)$	$(0_1 \ 1_0 \ 2_0)$

Fig. 6 Fuzzy texture unit of Fig.4(a)

Table 1 Texture unit number and its probability

TU	N	μ
2, 0, 1, 1, 0, 2, 0, 2	4898	0.1186
2, 0, 1, 2, 0, 2, 0, 2	4925	0.5278
2, 1, 1, 1, 0, 2, 0, 2	4901	0.0529
2, 0, 1, 2, 0, 2, 0, 2	4928	0.2557

According to the definition of nonlinear membership function, each fuzzy texture unit may have several different texture unit numbers. Because froth images are made up of many 3*3 areas, therefore, in accordance with the calculation of fuzzy texture spectrum in Fig.4(a), the frequency of various texture unit number can be obtained. Then FTS is the statistical histogram of the various texture unit numbers for all the fuzzy texture units.

4 Rotate classification fuzzy texture spectrum (RCFTS)

Although in a previews work^[28] we have proved the FTS is better than BTS in texture recognition. However the high dimension and the low efficiency is still an intractable problem. In recent researches, P. Gong^[33] proposed a simple way that combine the comparison of ‘greater’ and ‘equal’ into one ‘greater and equal’, which dramatically reduces the dimension from 6561 to 256. However, it is too simple to keep important details of the image.

Because the froth image has a simple background and the texture spectrum focus on the single pixel, so we take non directional texture into consideration. Then the TU could be simplified from 6561 to 834 classes without losing the texture information. In this case, the texture units in the same class are those who differing from each other only by rotation of 45 degree. To explain this concept, two of the classes are given in Fig.7.

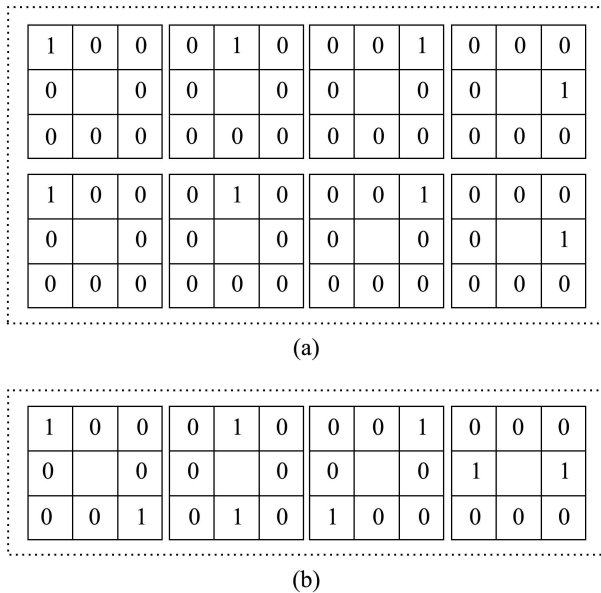


Fig. 7 Texture units in (a) belongs to class 1 and (b) belongs to class 82

5 Coarse and homogenous membership function obtaining

For detecting the classes standing for coarseness and homogeneity, as well as the degree to which a given images is coarse or homogeneous, we have analyzed the spectrum of the images looking for outstanding frequencies. We consider outstanding frequencies are those whose percentage with regard the total frequencies N (image height * width) is greater than one, because lower percentage values is significantly numerous rendering the calcu-

lation complex and irrelevant. According to the method above, and take Fig.3 for an example, four outstanding classes of texture units are coming up, they are O_7, O_8, Z_7, Z_8 with the frequency of $f_{O_7}, f_{O_8}, f_{Z_7}, f_{Z_8}$.

$$O_8 = \{\overline{11111111}\} = \{3280\},$$

$$O_7 = \{\overline{01111111}, \overline{11111112}\} = \{\overline{1093}, \overline{3281}\},$$

$$Z_7 = \{\overline{00000001}, \overline{12222222}\} = \{\overline{1}, \overline{4347}\},$$

$$Z_8 = \{\overline{00000000}, \overline{22222222}\} = \{\overline{0}, \overline{6560}\}.$$

To expatiate it, we choose a froth image in spot, and add three gradually increased white noise to the original image, getting four images, shown in Fig.8.

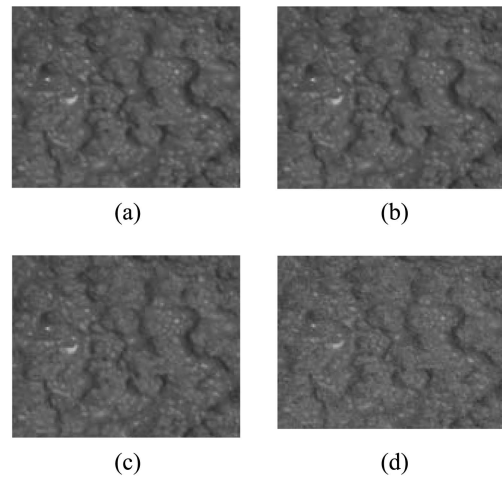


Fig. 8 Subset of froth images in order of noise degree

The frequencies of each image based on RCFTS are shown in Table 2.

Table 2 Frequencies of noise images

Images	f_{O_8}	f_{O_7}	f_{Z_8}	f_{Z_7}
(a)	51847	49446	—	—
(b)	50121	37632	—	—
(c)	36678	16607	21802	31237
(d)	—	—	40550	14331

According to Table 2, main rules are given as follows: $f_{O_7}, f_{O_8}, f_{Z_7}, f_{Z_8}$ Rule Coarse (1): The smaller f_{O_7}/f_{Z_8} is, the more Coarse is the image.

Rule Coarse (2): When $f_{O_7} < 0.01N$, μ_T is very large.

Rule Coarse (3): The greater the $f_{Z_7}+f_{Z_8}$ is, the more Coarse the image is.

Rule Homogenous (1): The smaller the f_{Z_8}/f_{O_7} is, the more Homogenous is the image.

Rule Homogenous (2): When $f_{Z_8} < 0.01N$, μ_H is very large.

Rule Homogenous (3): The greater the $f_{O_7}+f_{O_8}$ is, the more Homogenous the image is.

On the basis of these rules, the membership degrees of homogenous and texture, μ_T and μ_H is easy to get

$$\begin{cases} \mu_H = \max\{0, \min\{1, \frac{1}{2}(1 + o - z)\}\}, \\ \mu_T = \max\{0, \min\{1, \frac{1}{2} - 2 \cdot o + 2 \cdot z\}\}. \end{cases} \quad (6)$$

Where
$$o = \frac{f_{O_7} + f_{O_8}}{N}, z = \frac{f_{Z_7} + f_{Z_8}}{N}.$$

6 Results and discussion

Forty preprocessed froth images are acquired in spot under certain conditions for experiment. Four representative images of them are given, corresponding grade 12.51, 14.86, 15.73 and 10.77. Fig.9 shows the four froth images of 512×512 pixels, in which, 9(a) is obviously the smoothest, while (b)–(d) is more complex relatively.

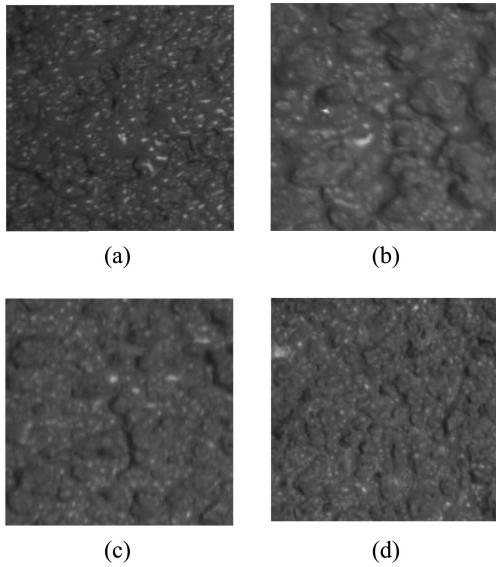


Fig. 9 Subset of froth images

Table 3 shows the results of Fig.9 using the formula above.

images	<i>o</i>	<i>z</i>	μ_H	grades
(a)	0.4563	0.0001	0.7280	12.51
(b)	0.3864	0.0004	0.6930	14.86
(c)	0.3540	0.0009	0.6765	15.73
(d)	0.3040	0.0001	0.6515	10.77

The calculation results shows that μ_H is quite large while μ_T is always negligible, so the value of μ_H is used to describe froth images. Values of μ_H in Fig.9 based on RCFTS is 0.7280, 0.6930, 0.6765 and 0.6515 in order, which means the image is getting more coarse. Therefore, the texture complexity based on RCFTS is able to describe froth images homogeneity and consistent with human vision perception. Meanwhile the considerable good grade of image (3) has a μ_H value of 0.68, and the concentrate grade turns lower no matter increases or decrease. So to acquire a more universal result, we draw Fig.10 of all the 40 images according to the concentration grade and μ_H .

Fig.10 shows the relationship of μ_H and grade. In general, the lower μ_H is, the higher the concentration grade is, and when the grade reaches a favorable degree between 14 and 16, μ_H is from 0.68 to 0.71. In addition, when μ_H of the fourth image is the smallest, its grade declines. Operation records shows this is because collector dosage

was too large, which led to too many mineral particles attaching in bubble surface. During the process that bubbles rise to the surface to form froth, the water between bubbles film is dropping back to pulp under the role of gravity, which causes the thin film and dry froth, consequently the froth bearing ability reduces. When the mineral content is beyond the bubbles bearing ability, the bubbles collapse. Then many mineral particles fall into the pulp resulting in coarse texture with small grade. Thus it is reliable and effective to reflect the concentrate grades in real time and coach the operation in the field using the homogeneity of the fourth image.

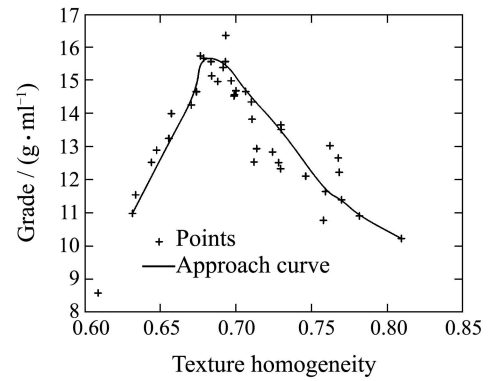


Fig. 10 Relationship between texture complexity and grade

7 Conclusions

The RCFTS based on non-linear membership function is able to describe the texture homogenous of froth images, and meanwhile accords with human visual perception. And compared to FTS, RCFTS method is quite efficient and effective. When it is difficult to extract the characteristics such as size, shape, velocity accurately, texture homogeneity as a novel characteristic is proved very efficient by presenting the relationship between texture character and mineral grade. Its prospect of popularization and application to other mineral flotation processes will be seen experimentally.

Meanwhile how to optimize the mineral separation and purification process in spot will be the further interesting investigation.

References:

- [1] SCHWARZ S, GRANO S. Effect of particle hydrophobicity on particle and water transport across a flotation froth [J]. *Colloids and Surfaces A: Physicochemical and Engineering Aspects*, 2005, 256(2/3): 157 – 164.
- [2] ALBIJANIC B, OZDEMIR O, NGUYEN A V, et al. A review of induction and attachment times of wetting thin films between air bubbles and particles and its relevance in the separation of particles by flotation [J]. *Advances in Colloid and Interface Science*, 2010, 159(1): 1 – 21.
- [3] MEHRABANI J V, NOAPARAST M, MOUSAVI S M, et al. Process optimization and modelling of sphalerite flotation from a low-grade Zn-Pb ore using response surface methodology [J]. *Separation and Purification Technology*, 2010, 72(3): 242 – 249.
- [4] MASSOLA C P, CHAVES A P, LIMA J R B, et al. Separation of silica from bauxite via froth flotation [J]. *Minerals Engineering*, 2009, 22(4): 315 – 318.
- [5] AL-SHAMRANI A A, JAMES A, XIAO H. Separation of oil from water by dissolved air flotation [J]. *Colloids and Surfaces A: Physicochemical and Engineering Aspects*, 2002, 209(1): 15 – 26.

- [6] LIU S, WANG Q, MA H, et al. Effect of micro-bubbles on coagulation flotation process of dyeing wastewater [J]. *Separation and Purification Technology*, 2010, 71(3): 337 – 346.
- [7] BONIFAZI G, MASSACCI P, MELONI A. A 3D froth surface rendering and analysis technique to characterize flotation processes [J]. *International Journal of Mineral Processing*, 2002, 64(2–3): 153 – 161.
- [8] PANDIT R B, TANG J, LIU F, et al. A computer vision method to locate cold spots in foods in microwave sterilization process [J]. *Pattern Recognition*, 2007, 40(12): 3667 – 3676.
- [9] TESSIER J, DUCHESNE C, BARTOLACCI G. A machine vision approach to on-line estimation of run-of-mine ore composition on conveyor belts [J]. *Minerals Engineering*, 2007, 20(12): 1129 – 1144.
- [10] KAARTINEN J, HATONENB J, HYÖTYNIEMI H, et al. Machine-vision-based control of zinc flotation—A case study [J]. *Control Engineering Practice*, 2006, 14(12): 1455 – 1466.
- [11] YANG C, XU C, GUI W, et al. Application of highlight removal and multivariate image analysis to color measurement of flotation bubble images [J]. *International Journal of Imaging Systems and Technology*, 2009, 19(4): 316 – 322.
- [12] REDDICK J F, HESKETH A H, MORAR S H, et al. An evaluation of factors affecting the robustness of colour measurement and its potential to predict the grade of flotation concentrate [J]. *Minerals Engineering*, 2009, 22(1): 64 – 69.
- [13] BONIFAZI G, SERRANTI S, VOLPE F, et al. Characterization of flotation froth colour and structure by machine vision [J]. *Computers & Geosciences*, 2005, 27(9): 1111 – 1117.
- [14] YANG C, XU C, MU X, et al. Bubble size estimation using interfacial morphological information for mineral flotation process monitoring [J]. *Transactions of Nonferrous Metals Society of China*, 2009, 19(3): 694 – 699.
- [15] ZHOU K, YANG C, GUI W, et al. Clustering-driven watershed adaptive segmentation of bubble image [J]. *Journal of Central South University of Technology*, 2010, 17(5): 1049 – 1057.
- [16] SUPOMO A, YAP E, ZHENG X, et al. PT Freeport Indonesia's mass-pull control strategy for rougher flotation [J]. *Minerals Engineering*, 2008, 21(12–14): 808 – 816.
- [17] BARBIAN N, HADLER K, VENTURA-MEDINA E, et al. The froth stability column: linking froth stability and flotation performance [J]. *Minerals Engineering*, 2005, 18(3): 317 – 324.
- [18] MORAR S H, HATFIELD D P, BARBIAN N, et al. A comparison of flotation froth stability measurements and their use in the prediction of concentrate grade [C] // *Proceedings of the XXIII International Minerals Processing Congress*. Istanbul, Turkey: [s.n.], 2006: 739 – 744.
- [19] BARBIAN N, CILLIERS J J, MORAR S H, et al. Froth imaging, air recovery and bubble loading to describe flotation bank performance [J]. *International Journal of Mineral Processing*, 2007, 84(1–4): 81 – 88.
- [20] BARTOLACCI G, PELLETIER JR P, TESSIER JR J, et al. Application of numerical image analysis to process diagnosis and physical parameter measurement in mineral processes—part I: flotation control based on froth textural characteristics [J]. *Minerals Engineering*, 2006, 19(6–8): 734 – 747.
- [21] SHEAN B J, CILLIERS J J. A review of froth flotation control [J]. *International Journal of Mineral Processing*, 2011, 100(3–4): 57 – 71.
- [22] HARGRAVE J M, HALL S T. Diagnosis of concentrate grade and mass flowrate in tin flotation from colour and surface texture analysis [J]. *Minerals Engineering*, 1997, 10(6): 613 – 621.
- [23] MARAIS C, ALDRICH C. Estimation of platinum flotation grades from froth image data [J]. *Minerals Engineering*, 2011, 24(5): 433 – 441.
- [24] ALDRICH C, FENG D. Effect of frothers on bubble size distributions in flotation pulp phases and surface froths [J]. *Minerals Engineering*, 2000, 13(10–11): 1049 – 1057.
- [25] HYÖTYNIEMI H, YLINEN R. Modeling of visual flotation froth data [J]. *Control Engineering Practice*, 2000, 8(3): 313 – 318.
- [26] HOLTHAM P N, NGUYEN K K. On-line analysis of froth surface in coal and mineral flotation using JKFFrothCam [J]. *International Journal of Mineral Processing*, 2002, 64(2–3): 163 – 180.
- [27] LIN B, RECKE B, KNUDSEN J K H, et al. Bubble size estimation for flotation processes [J]. *Minerals Engineering*, 2008, 21(7): 539 – 548.
- [28] CHENG C, YANG C, ZHOU K. Flotation froth image texture extraction method based on fuzzy texture [J]. *Mineral Engineering Research*, 2009, 24(4): 62 – 66.
- [29] BOUCHARD J, ANDRÉD, DEL VILLAR R, et al. Column flotation simulation and control: an overview [J]. *Minerals Engineering*, 2009, 22(6): 519 – 529.
- [30] ABRAMOV A, MAGAZANIK D V. Theoretical basis for optimal collector concentrations and pulp pH values during flotation of sulfide-free minerals [J]. *Journal of Mining Science*, 2006, 42(2): 178 – 188.
- [31] HE D C, WANG L. Unsupervised textural classification of image using the texture spectrum [J]. *Pattern Recognition*, 1992, 25(3): 247 – 255.
- [32] BARCELO A, MONTSENY E, SOBREVILLA P. Fuzzy texture unit and fuzzy texture spectrum for texture characterization [J]. *Fuzzy Sets and Systems*, 2007, 158(3): 239 – 252.
- [33] GONG P, MARCEAU D J, HOWARTH P J. A comparison of special feature extraction algorithms for land-use classification with SPOT HRV data [J]. *Remote Sensing of Environment*, 1992, (40): 137 – 151.

作者简介:

周璇 (1988–), 女, 硕士, 目前研究方向为图像处理与模式识别、图像纹理特征研究等, E-mail: zhoux316@126.com;

阳春华 (1965–), 女, 博士, 教授, 目前研究方向为复杂工业过程的建模与优化、实时系统容差计算等, E-mail: ychh@csu.edu.cn;

任会峰 (1981–), 男, 博士, 目前研究方向为图像处理与模式识别、基于视觉图像的软测量等, E-mail: renhf316@163.com;

陈志鹏 (1987–), 男, 硕士, 目前研究方向为图像处理, E-mail: 466628563@qq.com;

曾子骄 (1988–), 男, 硕士研究生, 目前研究方向为图像处理, E-mail: 239452054@qq.com.